

Isomerization dynamics of a buckled nanobeam

Peter Collins

School of Mathematics

University of Bristol

Bristol BS8 1TW

United Kingdom

Gregory S. Ezra*

Department of Chemistry and Chemical Biology

Baker Laboratory

Cornell University

Ithaca, NY 14853

USA

Stephen Wiggins[†]

School of Mathematics

University of Bristol

Bristol BS8 1TW

United Kingdom

(Dated: September 24, 2018)

Abstract

We analyze the dynamics of a model of a nanobeam under compression. The model is a two mode truncation of the Euler-Bernoulli beam equation subject to compressive stress applied at both ends. We consider parameter regimes where the first mode is unstable and the second mode can be either stable or unstable, and the remaining modes (neglected) are always stable. Material parameters used correspond to a silicon nanobeam. The two mode model Hamiltonian is the sum of a (diagonal) kinetic energy term and a potential energy term. The form of the potential energy function suggests an analogy with isomerisation reactions in chemistry, where ‘isomerisation’ here corresponds to a transition between two stable beam configurations. We therefore study the dynamics of the buckled beam using the conceptual framework established for the theory of isomerisation reactions. When the second mode is stable the potential energy surface has an index one saddle and when the second mode is unstable the potential energy surface has an index two saddle and two index one saddles. Symmetry of the system allows us to readily construct a phase space dividing surface between the two “isomers” (buckled states); we rigorously prove that, in a specific energy range, it is a normally hyperbolic invariant manifold. The energy range is sufficiently wide that we can treat the effects of the index one and index two saddles on the isomerisation dynamics in a unified fashion. We have computed reactive fluxes, mean gap times and reactant phase space volumes for three stress values at several different energies. In all cases the phase space volume swept out by isomerizing trajectories is considerably less than the reactant density of states, proving that the dynamics is highly nonergodic. The associated gap time distributions consist of one or more ‘pulses’ of trajectories. Computation of the reactive flux correlation function shows no sign of a plateau region; rather, the flux exhibits oscillatory decay, indicating that, for the 2-mode model in the physical regime considered, a rate constant for isomerization does not exist.

PACS numbers: 05.45.-a, 62.25.Fg, 62.25.-g, 82.20.-w, 82.20.Pm, 82.20.Sb, 82.20.Db, 83.10.Ff, 89.90.+n

I. INTRODUCTION

There is currently much interest in the mechanical properties of nanoscale objects such as rods and cantilevers¹⁻⁴. For example, changes in resonant frequencies with mass loading can enable sensitive detection of molecular species with given mass. The possible manifestation of quantum effects are also of great interest (see ref. 5 for a recent review). The effects of mechanical stress on nanostructures, such as the buckling of nanobeams, has been studied both experimentally and theoretically⁶⁻⁸. This latter work is directly related to the work in this paper.

The system studied in the present paper is a nanobeam subject to compressive stress. According to standard continuum mechanics, the beam will buckle as the magnitude of the associated compressive strain increases. More specifically, following previous work⁹⁻¹¹, we consider a regime in which the dynamics of the buckled beam is usefully described by a 2-mode model obtained by truncation of the full dynamics. In the regime considered, one of the modes is always unstable, while the second mode can be either stable or unstable, and all remaining modes (which are not considered explicitly) are stable.

We derive a 2 degree-of-freedom (DoF) Hamiltonian describing the 2-mode dynamics. The Hamiltonian describes a bistable (reactive) mode coupled to a transverse degree of freedom; the dynamical system thereby obtained has precisely the form of simple model potentials that have been used to describe isomerization reactions in chemistry¹²⁻²⁰. However, for the nanobeam problem, the simple form of the potential is a rigorous consequence of the 2-mode truncation of the dynamics rather than an approximation to an unknown molecular potential energy function.

We can therefore investigate the dynamics of the buckled nanobeam using the conceptual framework established for the theory of isomerization reactions. A number of approaches to the study of isomerization dynamics have been developed in the chemical literature (see, for example, refs 16-18,20,21). Some basic relevant questions are the following: can ‘isomerization’ of the nanobeam be characterized by a *rate*? If so, can the rate coefficient be predicted using standard (so-called statistical) theories^{16,17,20}, such as transition state theory^{12,13,20,22,23}? If not, what are the dynamical properties of the system that lead to non-statistical reaction dynamics?

Chakraborty et al. have previously applied harmonic transition state theory (TST) to

predict isomerization rates for various nanobeams under compressive stress^{9–11}. The rates obtained using basic harmonic TST are proportional to the inverse of the curvature of the potential transverse to the reaction coordinate, and so diverge at the strain value for which the second mode passes from being stable to unstable (and the associated saddle point passes from being index 1 to index 2^{24–27}). Chakraborty has also applied a quantum version of harmonic TST to the nanobeam isomerization kinetics^{9–11}.

In the present paper we examine the dynamics of a compressed buckled Silicon (Si) nanobeam from the perspective of reaction rate theory. The potential function which emerges from a standard modal analysis of the transverse beam displacements has a high degree of symmetry, and the appropriate dividing surface for computation of reactive flux is then in fact completely determined by symmetry. Moreover, we are able to rigorously prove that the dividing surface is a normally hyperbolic invariant manifold in a specific energy range. The energy range is sufficient for treating the effects of the index one and index two saddles on the isomerisation dynamics in a unified fashion.

We compute both the distribution of gap times and the reactive flux at a number of energies in a physically relevant range. Our results show that, in this regime for the Si nanobeam considered: (i) the isomerization dynamics is extremely regular and nonergodic, and (ii) a rate constant for isomerization does not exist. Rather than exhibiting a rapid drop to a ‘plateau’ value followed by slow exponential decay^{14,16,19}, the reactive flux shows damped oscillatory decay. The system considered is in a regime ($T \gtrsim 100$ K) where quantum effects are likely to be negligible.

The structure of the paper is as follows. In Sec. II we derive the equations of motion for the nanobeam. In Sec. III we discuss in further detail the two degree-of-freedom Hamiltonian system obtained for the 2-mode truncation of the beam dynamics. Particular attention is given to the phase space geometry, specifically, the existence of a normally hyperbolic invariant manifold (NHIM)²⁸ in the system phase space. In Sec. IV we review some concepts from reaction rate theory: phase space dividing surfaces and volumes, gap times and reactive fluxes. In Sec. V we discuss the physical parameter values and energy scales appropriate to our calculations. Sec. VI presents the results of our numerical calculations, and Sec. VII concludes. In Appendix A we apply the concept of exponential dichotomies²⁹ to provide a proof of the existence of a NHIM in the phase space of the truncated nanobeam problem.

II. EQUATIONS OF MOTION FOR THE NANOBEAM

In this section we derive a 2-mode (classical) model for an Euler-Bernoulli beam subject to compressive stress applied at both ends. The derivation of the Euler-Bernoulli equations can be found in many textbooks on continuum mechanics (e.g. ref. 4). Our derivation and notation closely follows that of refs 9–11 (see also refs 6–8). A useful discussion of the concept of stress in a quantum mechanical system is given in ref. 30.

We consider an Euler-Bernoulli model of a beam of length L having width w and thickness d , where $L \gg w > d$. The requirement $w > d$ allows us to assume that transverse displacements, $y(x, t)$, occur only in the d direction. The linear modulus F (dimensions of energy per unit length) is related to the elastic modulus Q by $F = Qwd$. For a beam of rectangular cross-section the bending moment is given by $\kappa = \frac{d^2}{12}$ and $\mu = \frac{m}{L}$ denotes the mass per unit length. The length of the uncompressed rod is denoted by L_0 .

Constant compressive stress is applied to both ends of the beam, reducing the horizontal distance between the two endpoints of the beam to $L < L_0$. The strain ϵ is $\epsilon = \frac{L-L_0}{L_0}$, and is negative for compression. The compression causes a contribution to the potential energy of the beam due to bending in the d direction (the first term in (2.1)) and elasticity (the last three terms in (2.1)), where the potential energy has the form:

$$V[y(x, t)] = \frac{1}{2} \int_0^L dx (F\kappa^2(y'')^2 + F\epsilon(y')^2) + \frac{F}{8L_0} \left(\int_0^L dx (y')^2 \right)^2 + \frac{FL_0}{2} \epsilon^2. \quad (2.1)$$

The kinetic energy is:

$$T[\dot{y}(x, t)] = \frac{1}{2} \int_0^L dx \mu \dot{y}^2 \quad (2.2)$$

Forming the Lagrangian in the usual manner:

$$L[y(x, t), \dot{y}(x, t)] = T[\dot{y}(x, t)] - V[y(x, t)] \quad (2.3)$$

Lagrange's equations of motion are given by:

$$\frac{d}{dt} \frac{\delta L}{\delta \dot{y}} - \frac{\delta L}{\delta y} = 0. \quad (2.4)$$

Using (2.1) and (2.2), we have:

$$\frac{\delta T[\dot{y}(x, t)]}{\delta \dot{y}(x, t)} = \mu \dot{y}, \quad (2.5a)$$

$$\frac{\delta V[y(x, t)]}{\delta y(x, t)} = F\kappa^2 y^{[4]} - \left[F\epsilon y'' + \frac{F}{2L_0} \left(\int_0^L dx (y')^2 \right) y'' \right]. \quad (2.5b)$$

Using these expressions, together with (2.3) and (2.4), gives the equations of motion:

$$\mu \ddot{y} = -F\kappa^2 y^{[4]} + \left[F\epsilon y'' + \frac{F}{2L_0} \left(\int_0^L dx (y')^2 \right) y'' \right], \quad (2.6)$$

and the boundary conditions are chosen to be:

$$y(0, t) = y(L, t) = 0, \quad (2.7a)$$

$$y''(0, t) = y''(L, t) = 0, \quad (2.7b)$$

which are referred to in the literature as *hinged* boundary conditions.

One easily sees by inspecting (2.6) that $y(x, t) = 0$ is a solution. Linearizing (2.6) about this solution gives:

$$\mu \ddot{y} = -F\kappa^2 y^{[4]} + F\epsilon y''. \quad (2.8)$$

We seek the normal modes (eigenfunctions) of these linearized equations by assuming a solution of the form:

$$y_n(x, t) = y_n(x) e^{i\omega_n t}, \quad n = 1, 2, 3, \dots \quad (2.9)$$

where

$$y_n(x) = \sqrt{\frac{2}{L}} \sin \left[\frac{n\pi x}{L} \right]. \quad (2.10)$$

Note that the $y_n(x)$ satisfy the normalization condition:

$$\int_0^L y_n(x) y_m(x) dx = \delta_{n,m}. \quad (2.11)$$

Substituting (2.9) into (2.8) gives:

$$\mu \omega_n^2 y_n(x) = F\kappa^2 y_n^{[4]}(x) - F\epsilon y_n''(x) \quad (2.12)$$

We substitute (2.10) into (2.12), and after some algebra we obtain:

$$\omega_n = \omega_0 n \sqrt{n^2 - \frac{\epsilon}{\bar{\epsilon}}} \quad (2.13)$$

with

$$\omega_0 = \pi^2 \frac{\kappa}{L^2} \sqrt{\frac{F}{\mu}} \quad (2.14a)$$

$$\bar{\epsilon} = -\frac{\kappa^2 \pi^2}{L^2}. \quad (2.14b)$$

Note that the quantity $\bar{\epsilon}$ is approximately equal to the critical value of the strain ϵ_c , obtained by solving the implicit equation (2.14b), but has a weak dependence on ϵ .

From the form of (2.9) and (2.13), we see that the mode $y_n(x, t)$ is linearly stable (resp., unstable) provided $n^2 - \frac{\epsilon}{\bar{\epsilon}} > 0$ (resp., $n^2 - \frac{\epsilon}{\bar{\epsilon}} < 0$).

We will examine the situation where:

$$1 - \frac{\epsilon}{\bar{\epsilon}} < 0, \quad (2.15a)$$

$$4 - \frac{\epsilon}{\bar{\epsilon}} > 0 \quad \text{or} \quad 4 - \frac{\epsilon}{\bar{\epsilon}} < 0, \quad (2.15b)$$

$$n^2 - \frac{\epsilon}{\bar{\epsilon}} > 0, \quad n \geq 3. \quad (2.15c)$$

In other words, we will consider the cases where the first mode is always unstable, the second mode can be either stable or unstable, and modes $n \geq 3$ are all stable.

Assuming that the solution of (2.6) has the form:

$$y(x, t) = \sqrt{\frac{2}{L}} \sum_{n=1}^{\infty} A_n(t) \sin \left[\frac{n\pi x}{L} \right], \quad (2.16)$$

we substitute into (2.6) to obtain an infinite set of ordinary differential equations for the time evolution of the modal amplitudes, $A_n(t)$. However, we will simplify the problem by only considering the evolution of the first two modes:

$$y(x, t) = \sqrt{\frac{2}{L}} A_1(t) \sin \left[\frac{\pi x}{L} \right] + \sqrt{\frac{2}{L}} A_2(t) \sin \left[\frac{2\pi x}{L} \right]. \quad (2.17)$$

In this case one obtains a two-degree-of-freedom system for the evolution of the modal amplitudes $A_1(t)$ and $A_2(t)$. Defining momentum variables $p_i = \mu \dot{A}_i$, $i = 1, 2$, the time evolution of the amplitudes A_i is described by a two degree-of-freedom Hamiltonian system, with Hamiltonian:

$$H = \frac{p_1^2}{2\mu} + \frac{p_2^2}{2\mu} + V(A_1, A_2), \quad (2.18)$$

where the potential energy has the form:

$$V(A_1, A_2) = \frac{F\pi^2(\epsilon - \bar{\epsilon})}{2L^2} A_1^2 + \frac{2F\pi^2(\epsilon - 4\bar{\epsilon})}{L^2} A_2^2 + \frac{F\pi^4}{8L^4 L_0} (A_1^2 + 4A_2^2)^2. \quad (2.19)$$

It is natural to ask how well the two-mode truncation described by the two degree-of-freedom Hamiltonian system defined by Hamiltonian (2.18) models the solution of the full partial differential equation describing the Euler-Bernoulli beam given in (2.6). It is a standard engineering approximation to approximate the full solution of a partial differential

equation by considering a truncated modal expansion of eigenfunctions obtained from the linearized equations about an equilibrium state. The reasoning is that the evolution near the equilibrium solution is dominated by the evolution of the unstable modes. In some cases this can be rigorously proven using center manifold or inertial manifold techniques (see, e.g., refs 31,32). A seminal example of this approach that played a fundamental role in the development of applied dynamical systems theory was the work of Holmes, Marsden, and Moon on the dynamics of a buckled beam subject to periodic (temporal) forcing^{33–35}. Initially, a combination of experimental and theoretical work showed that the experimentally observed chaotic behavior was captured by the evolution of the one unstable mode, subject to forcing^{33,34}. Later, it was rigorously shown³⁵ that this single mode truncation captured the dynamics of the full partial differential equation governing the beam (near the instability). In this paper we will not be concerned with these issues. Rather, we take as the starting point of our analysis the two degree-of-freedom Hamiltonian system governing the two mode truncation of the Euler-beam equation given in (2.6).

III. TWO-MODE TRUNCATION: HAMILTONIAN AND PHASE SPACE GEOMETRY

We begin by non-dimensionalizing the two degree-of-freedom Hamiltonian system of eq. (2.18). Defining the dimensionless amplitudes:

$$A_1 = \frac{L\sqrt{2L_0}}{\pi} \bar{A}_1, \quad (3.1a)$$

$$A_2 = \frac{L\sqrt{2L_0}}{\pi} \bar{A}_2 \quad (3.1b)$$

and substituting these expressions into the potential function (2.19) gives:

$$V(\bar{A}_1, \bar{A}_2) = FL_0 \left[(\epsilon - \bar{\epsilon})\bar{A}_1^2 + (\epsilon - 4\bar{\epsilon})4\bar{A}_2^2 + \frac{1}{2}(\bar{A}_1^2 + 4\bar{A}_2^2)^2 \right] \quad (3.2a)$$

$$\equiv FL_0 \bar{V}(\bar{A}_1, \bar{A}_2). \quad (3.2b)$$

Defining associated momenta $\{\bar{p}_k\}$ conjugate to the $\{\bar{A}_k\}$ via

$$\bar{p}_1 = \frac{L\sqrt{2L_0}}{\pi} p_1, \quad (3.3a)$$

$$\bar{p}_2 = \frac{L\sqrt{2L_0}}{\pi} p_2 \quad (3.3b)$$

and substituting into (2.18) gives the scaled Hamiltonian:

$$\bar{H} \equiv \frac{H}{FL_0} = \frac{\bar{p}_1^2}{2\bar{\mu}} + \frac{\bar{p}_2^2}{2\bar{\mu}} + \bar{V}(\bar{A}_1, \bar{A}_2) \quad (3.4)$$

where

$$\bar{\mu} \equiv \mu \frac{2FL^2L_0^2}{\pi^2} \quad (3.5)$$

Rescaling the momenta

$$\bar{p}_i \rightarrow \frac{\bar{p}_i}{\bar{\mu}^{1/2}}, \quad i = 1, 2 \quad (3.6)$$

we obtain the following Hamiltonian:

$$\bar{H} = \frac{\bar{p}_1^2}{2} + \frac{\bar{p}_2^2}{2} + \bar{V}(\bar{A}_1, \bar{A}_2), \quad (3.7)$$

with

$$\bar{V}(\bar{A}_1, \bar{A}_2) = \alpha \bar{A}_1^2 + 4\beta \bar{A}_2^2 + \frac{1}{2}(\bar{A}_1^2 + 4\bar{A}_2^2)^2, \quad (3.8)$$

and

$$\alpha = \epsilon - \bar{\epsilon} \quad (3.9a)$$

$$\beta = \epsilon - 4\bar{\epsilon}. \quad (3.9b)$$

The corresponding Hamiltonian equations of motion (for suitably rescaled time) are then:

$$\dot{\bar{A}}_1 = \frac{\partial \bar{H}}{\partial \bar{p}_1} = \bar{p}_1, \quad (3.10a)$$

$$\dot{\bar{p}}_1 = -\frac{\partial \bar{H}}{\partial \bar{A}_1} = -2\bar{A}_1 (\alpha + \bar{A}_1^2 + 4\bar{A}_2^2), \quad (3.10b)$$

$$\dot{\bar{A}}_2 = \frac{\partial \bar{H}}{\partial \bar{p}_2} = \bar{p}_2, \quad (3.10c)$$

$$\dot{\bar{p}}_2 = -\frac{\partial \bar{H}}{\partial \bar{A}_2} = -8\bar{A}_2 (\beta + \bar{A}_1^2 + 4\bar{A}_2^2). \quad (3.10d)$$

A. Equilibria and their stability

From the (algebraically) simple form of Hamilton's equations given in eq. (3.10) it is straightforward to compute the equilibria, determine their linearized stability properties (i.e. compute the eigenvalues of the matrix associated with the linearization of Hamilton's equations about the equilibrium point), and compute the (total) energy of the equilibrium point. These properties are summarized in Table I.

For $\alpha < 0$, $\beta > 0$ there are only three equilibrium points. The origin is an index one saddle point and the remaining two equilibria have two pairs of purely imaginary eigenvalues (minima of the potential (3.8)). For $\alpha < 0$, $\beta < 0$, $|\alpha| > |\beta|$, the origin is an index two saddle, phase space points $(\bar{A}_1, \bar{p}_1, \bar{A}_2, \bar{p}_2) = (\pm\sqrt{-\alpha}, 0, 0, 0)$ have two pairs of purely imaginary eigenvalues and correspond to minima of the potential (3.8), and $(\bar{A}_1, \bar{p}_1, \bar{A}_2, \bar{p}_2) = (0, 0, \pm\frac{\sqrt{-\beta}}{2}, 0)$ are index one saddles.

B. Invariant planes and the existence of a Normally Hyperbolic Invariant Manifold

It can be seen by inspection of (3.10) that, if we set $\bar{A}_2 = \bar{p}_2 = 0$ (resp., $\bar{A}_1 = \bar{p}_1 = 0$), then $\dot{\bar{A}}_2 = \dot{\bar{p}}_2 = 0$ (resp., $\dot{\bar{A}}_1 = \dot{\bar{p}}_1 = 0$). It then follows that the two planes:

$$\Pi_1 = \{(\bar{A}_1, \bar{p}_1, \bar{A}_2, \bar{p}_2) \mid \bar{A}_2 = \bar{p}_2 = 0\}, \quad (3.11a)$$

$$\Pi_2 = \{(\bar{A}_1, \bar{p}_1, \bar{A}_2, \bar{p}_2) \mid \bar{A}_1 = \bar{p}_1 = 0\} \quad (3.11b)$$

are each invariant with respect to the dynamics generated by (3.10). The dynamics on Π_1 is given by the Hamiltonian system defined by the Hamiltonian

$$\bar{H}_1 \equiv \frac{\bar{p}_1^2}{2} + \alpha \bar{A}_1^2 + \frac{1}{2} \bar{A}_1^4 \quad (3.12a)$$

and the dynamics on Π_2 is given by the Hamiltonian system defined by the Hamiltonian

$$\bar{H}_2 \equiv \frac{\bar{p}_2^2}{2} + 4\beta\bar{A}_2^2 + 8\bar{A}_2^4. \quad (3.12b)$$

Hence, the dynamics on each plane is integrable. However, the dynamics on each plane is *not* isoenergetic. The three dimensional energy surface intersects a two dimensional plane in the four dimensional phase space in a one dimensional set, i.e. a trajectory of the one degree-of-freedom Hamiltonian system defined by \bar{H}_1 (for intersections with Π_1) or a trajectory of the one degree-of-freedom Hamiltonian system defined by \bar{H}_2 (for intersections with Π_2).

We now want to determine conditions under which some portion of Π_2 is a normally hyperbolic invariant manifold (NHIM). Roughly speaking, NHIMs have saddle-like stability properties in directions transverse to the invariant manifolds²⁸. In recent years NHIMs have been shown to be a significant phase space structure related to reaction dynamics. For example, they play the key role in the construction of a phase space dividing surface having the no-recrossing property^{36,37} and minimal flux³⁸. They have also been shown to be central to Thiele's theory³⁹ of reaction dynamics in terms of gap times²¹.

The following theorem provides sufficient conditions for the existence of a NHIM (the proof is given in Appendix A):

Theorem 1 *Consider $\alpha < 0$ and the region on the Π_2 plane bounded by the curve:*

$$\frac{\bar{p}_2^2}{2} + 4\beta\bar{A}_2^2 + 8\bar{A}_2^4 = E_{max}, \quad (3.13)$$

where

$$E_{max} = \frac{\alpha^2}{2} \left(1 - 2\frac{\beta}{\alpha} \right). \quad (3.14)$$

Then this region on Π_2 is a two-dimensional (non-isoenergetic) normally hyperbolic invariant manifold.

Note that for a given three dimensional energy surface the NHIM is a (one dimensional) trajectory on Π_2 .

C. The existence of a phase space dividing surface having the no-recrossing property

For the Hamiltonian (3.7) we now construct a dividing surface in phase space having the “no-recrossing” property. We will describe what this means, as well as the dynamical

significance of the dividing surface, in the course of our construction.

The codimension one non-isoenergetic surface defined by $\bar{A}_1 = 0$ divides the phase space into two regions: one associated with the potential well whose minimum is $(\bar{A}_1, \bar{p}_1, \bar{A}_2, \bar{p}_2) = (\sqrt{-\alpha}, 0, 0, 0)$ and the other associated with the potential well whose minimum is $(\bar{A}_1, \bar{p}_1, \bar{A}_2, \bar{p}_2) = (-\sqrt{-\alpha}, 0, 0, 0)$. The dividing surface restricted to a fixed energy surface $\bar{H} = E$ is given by:

$$DS(E) = \left\{ (\bar{A}_1, \bar{p}_1, \bar{A}_2, \bar{p}_2) \mid \bar{A}_1 = 0, \bar{H} = \frac{\bar{p}_1^2}{2} + \frac{\bar{p}_2^2}{2} + 4\beta\bar{A}_2^2 + 8\bar{A}_2^4 = E \right\} \quad (3.15)$$

This dividing surface has two halves:

$$DS_+(E) = \left\{ (\bar{A}_1, \bar{p}_1, \bar{A}_2, \bar{p}_2) \mid \bar{A}_1 = 0, \bar{H} = \frac{\bar{p}_1^2}{2} + \frac{\bar{p}_2^2}{2} + 4\beta\bar{A}_2^2 + 8\bar{A}_2^4 = E, \bar{p}_1 > 0 \right\} \quad (3.16a)$$

and

$$DS_-(E) = \left\{ (\bar{A}_1, \bar{p}_1, \bar{A}_2, \bar{p}_2) \mid \bar{A}_1 = 0, \bar{H} = \frac{\bar{p}_1^2}{2} + \frac{\bar{p}_2^2}{2} + 4\beta\bar{A}_2^2 + 8\bar{A}_2^4 = E, \bar{p}_1 < 0 \right\}. \quad (3.16b)$$

These two halves meet at the NHIM:

$$\text{NHIM}(E) = \left\{ (\bar{A}_1, \bar{p}_1, \bar{A}_2, \bar{p}_2) \mid \bar{A}_1 = 0, \bar{H} = \frac{\bar{p}_2^2}{2} + 4\beta\bar{A}_2^2 + 8\bar{A}_2^4 = E, \bar{p}_1 = 0 \right\}. \quad (3.17)$$

The nature of the NHIM (i.e., the boundary between $DS_+(E)$ and $DS_-(E)$) depends on both E and β . The dynamics on the $\bar{A}_2 - \bar{p}_2$ plane is illustrated in Fig. 1.

We now argue that $DS_+(E)$ and $DS_-(E)$ are surfaces having the no (local) re-crossing property. These surfaces are defined by $\bar{A}_1 = 0$. Therefore points on these surfaces leave if $\dot{\bar{A}}_1 \neq 0$. We see from (3.10) that $\dot{\bar{A}}_1 = \frac{\partial \bar{H}}{\partial \bar{p}_1} = \bar{p}_1$. Therefore on $DS_+(E)$ we have $\dot{\bar{A}}_1 > 0$ and on $DS_-(E)$ we have $\dot{\bar{A}}_1 < 0$. Trajectories through points on $DS_+(E)$ move towards the region of phase space associated with the potential well whose minimum is $(\bar{A}_1, \bar{p}_1, \bar{A}_2, \bar{p}_2) = (\sqrt{-\alpha}, 0, 0, 0)$ and points on $DS_-(E)$ move towards the region of phase space associated with the potential well whose minimum is $(\bar{A}_1, \bar{p}_1, \bar{A}_2, \bar{p}_2) = (-\sqrt{-\alpha}, 0, 0, 0)$.

We denote the directional flux across these hemispheres by $\phi_+(E)$ and $\phi_-(E)$, respectively, and note that $\phi_+(E) + \phi_-(E) = 0$. The magnitude of the flux is $|\phi_+(E)| = |\phi_-(E)| \equiv \phi(E)$. The magnitude of the flux and related quantities are central to the theory of isomerization rates, as discussed in Sec. IV.

IV. PHASE SPACE VOLUMES, GAP TIMES, AND REACTIVE FLUX

In this section we briefly review the concepts from classical reaction rate theory that will be applied to the dynamics of the buckled nanobeam.

Points in the 4-dimensional system phase space $\mathcal{M} = \mathbb{R}^4$ are denoted $\mathbf{z} \equiv (\bar{p}_1, \bar{p}_2, \bar{A}_1, \bar{A}_2) \equiv (\bar{\mathbf{p}}, \bar{\mathbf{A}}) \in \mathcal{M}$. The system Hamiltonian is $\bar{H}(\mathbf{z})$, and the 3 dimensional energy shell at energy E , $\bar{H}(\mathbf{z}) = E$, is denoted $\Sigma_E \subset \mathcal{M}$. The corresponding microcanonical phase space density is $\delta(E - \bar{H}(\mathbf{z}))$, and the associated density of states for the complete energy shell at energy E is

$$\rho(E) = \int_{\mathcal{M}} d\mathbf{z} \delta(E - \bar{H}(\mathbf{z})). \quad (4.1)$$

The disjoint regions of phase space separated by $\text{DS}(E)$ are denoted \mathcal{M}_{\pm} ; the region of phase space corresponding to the potential well whose minimum is $(\bar{A}_1, \bar{p}_1, \bar{A}_2, \bar{p}_2) = (\sqrt{-\alpha}, 0, 0, 0)$ will be denoted by \mathcal{M}_+ , and that corresponding to the potential well whose minimum is $(\bar{A}_1, \bar{p}_1, \bar{A}_2, \bar{p}_2) = (-\sqrt{-\alpha}, 0, 0, 0)$ will be denoted by \mathcal{M}_- .

The microcanonical density of states for points in region \mathcal{M}_+ is

$$\rho_+(E) = \int_{\mathcal{M}_+} d\mathbf{z} \delta(E - H(\mathbf{z})) \quad (4.2)$$

with a corresponding expression for the density of states $\rho_-(E)$ in \mathcal{M}_- . Since the flow is everywhere transverse to $\text{DS}_{\pm}(E)$, those phase points in the region \mathcal{M}_+ that lie on crossing trajectories^{15,16} (i.e., those trajectories that cross $\text{DS}_{\pm}(E)$) can be specified uniquely by coordinates $(\tilde{p}, \tilde{A}, \psi)$, where $(\tilde{p}, \tilde{A}) \in \text{DS}_+(E)$ is a point on $\text{DS}_+(E)$, specified by 2 coordinates (\tilde{p}, \tilde{A}) , and ψ is a time variable. The point $\mathbf{z}(\tilde{p}, \tilde{A}, \psi)$ is reached by propagating the initial condition $(\tilde{p}, \tilde{A}) \in \text{DS}_+(E)$ forward for time ψ ^{21,39}. As all initial conditions on $\text{DS}_+(E)$ (apart from a set of trajectories of measure zero lying on stable manifolds) will leave the region \mathcal{M}_+ in finite time by crossing $\text{DS}_-(E)$, for each $(\tilde{p}, \tilde{A}) \in \text{DS}_+(E)$, we can define the *gap time* $s = s(\tilde{p}, \tilde{A})$, which is the time it takes for the trajectory to traverse the region \mathcal{M}_+ before entering the region \mathcal{M}_- . That is, $\mathbf{z}(\tilde{p}, \tilde{A}, \psi = s(\tilde{p}, \tilde{A})) \in \text{DS}_-(E)$. For the phase point $\mathbf{z}(\tilde{p}, \tilde{A}, \psi)$, we therefore have $0 \leq \psi \leq s(\tilde{p}, \tilde{A})$.

The coordinate transformation $\mathbf{z} \rightarrow (E, \psi, \tilde{p}, \tilde{A})$ is canonical³⁹⁻⁴², so that the phase space volume element is

$$d^4\mathbf{z} = dE d\psi d\sigma \quad (4.3)$$

with $d\sigma \equiv d\tilde{p} d\tilde{A}$ an element of 2 dimensional area on the $\text{DS}(E)$.

The magnitude $\phi(E)$ of the flux through dividing surface $\text{DS}_+(E)$ at energy E is given by

$$\phi(E) = \left| \int_{\text{DS}_+(E)} d\sigma \right|, \quad (4.4)$$

where the element of area $d\sigma$ is precisely the restriction to $\text{DS}(E)$ of the appropriate flux 2-form ω corresponding to the Hamiltonian vector field associated with $\bar{H}(\mathbf{z})$ ^{38,43–45}. The reactant phase space volume occupied by points initiated on the dividing surface with energies between E and $E + dE$ is therefore^{21,39,41,42,46–49}

$$dE \int_{\text{DS}_+(E)} d\sigma \int_0^s d\psi = dE \int_{\text{DS}_+(E)} d\sigma s \quad (4.5a)$$

$$= dE \phi(E) \bar{s} \quad (4.5b)$$

where the *mean gap time* \bar{s} is defined as

$$\bar{s} = \frac{1}{\phi(E)} \int_{\text{DS}_+(E)} d\sigma s \quad (4.6)$$

and is a function of energy E . The reactant density of states $\rho_+^{\text{C}}(E)$ associated with crossing trajectories only (those trajectories that enter and exit the region \mathcal{M}_+ ¹⁶) is then

$$\rho_+^{\text{C}}(E) = \phi(E) \bar{s} \quad (4.7)$$

where the superscript C indicates the restriction to crossing trajectories. The result (4.7) is essentially the content of the so-called classical spectral theorem^{41,42,46–49}.

If *all* points in the region \mathcal{M}_+ eventually leave that region (that is, all points lie on crossing trajectories^{15,16}) then

$$\rho_+^{\text{C}}(E) = \rho_+(E), \quad (4.8)$$

so that the crossing density of states is equal to the full reactant phase space density of states. Apart from a set of measure zero, all phase points $\mathbf{z} \in \mathcal{M}_+$ can be classified as either trapped (T) or crossing (C)¹⁶. A phase point in the trapped region \mathcal{M}_+^{T} never crosses the $\text{DS}(E)$, so that the associated trajectory does not contribute to the reactive flux. Phase points in the crossing region \mathcal{M}_+^{C} do however eventually cross the dividing surface, and so lie on trajectories that contribute to the reactive flux. In general, however, as a consequence of the existence of trapped trajectories (either trajectories on invariant *trapped* 2-tori^{15,16} or trajectories asymptotic to other invariant objects of zero measure), we have the inequality^{16,39,50}

$$\rho_+^{\text{C}}(E) \leq \rho_+(E). \quad (4.9)$$

If $\rho_+^C(E) < \rho_+(E)$, then it is in principle necessary to introduce corrections to statistical estimates of reaction rates^{16,18,50–53}. Numerical computation of crossing and reactive densities of states for the HCN molecule are discussed in refs 21,48,54, and results for the Hamiltonian isokinetic thermostat are discussed in ref. 55. Note that, if the strict inequality $\rho_+^C(E) < \rho_+(E)$ holds, then the system dynamics *cannot* be ergodic on the energy shell at energy E . The equality $\rho_+^C(E) = \rho_+(E)$ is therefore a necessary condition for ergodicity, one that can be checked numerically.

A. Gap time and reactant lifetime distributions

The *gap time distribution*, $\mathcal{P}(s; E)$ is of central interest in unimolecular kinetics^{39,56}: the probability that a phase point on $\text{DS}_+(E)$ at energy E has a gap time between s and $s + ds$ is equal to $\mathcal{P}(s; E)ds$. An important idealized gap distribution is the random, exponential distribution

$$\mathcal{P}(s; E) = k(E) e^{-k(E)s} \quad (4.10)$$

characterized by a single decay constant k (where k depends on energy E), with corresponding mean gap time $\bar{s} = k^{-1}$. An exponential distribution of gap times is usually taken to be a necessary condition for ‘statistical’ behavior in unimolecular reactions^{39,56–59}.

The lifetime (time to cross the dividing surface $\text{DS}_-(E)$) of phase point $\mathbf{z}(\tilde{p}, \tilde{A}, \psi)$ is $t = s(\tilde{p}, \tilde{A}) - \psi$, and the corresponding (normalized) reactant lifetime distribution function $\mathbb{P}(t; E)$ at energy E is^{39,56–58,60–62}

$$\mathbb{P}(t; E) = -\frac{d}{dt'} \text{Prob}(t \geq t'; E) \Big|_{t'=t} \quad (4.11a)$$

$$= \frac{1}{\bar{s}} \int_t^{+\infty} ds \mathcal{P}(s; E) \quad (4.11b)$$

where the fraction of interesting (reactive) phase points having lifetimes between t and $t + dt$ is $\mathbb{P}(t; E)dt$. It is often useful to work with the unnormalized lifetime distribution F , where $F(t; E) \equiv \bar{s} \mathbb{P}(t; E)$.

Equation (4.11a) gives the general relation between the lifetime distribution and the fraction of trajectories having lifetimes greater than a certain value for arbitrary ensembles^{60–62}. Note that an exponential gap distribution (4.10) implies that the reactant lifetime distribution $\mathbb{P}(t; E)$ is also exponential^{39,56,57,60–62}; both gap and lifetime distributions for realistic

molecular potentials have been of great interest since the earliest days of trajectory simulations of unimolecular decay, and many examples of non-exponential lifetime distributions have been found^{52,60–67}.

B. Reaction rates and the inverse gap time

The quantity

$$k_f^{\text{RRKM}}(E) \equiv \frac{\phi(E)}{\rho_+(E)} \quad (4.12)$$

is the statistical (RRKM) microcanonical rate for the forward reaction (trajectories crossing DS_+) at energy E , the ratio of the magnitude of the flux $\phi(E)$ through $\text{DS}_+(E)$ to the total reactant density of states^{12,68}.

Clearly, if $\rho_+(E) = \rho_+^{\text{C}}(E)$, then

$$k_f^{\text{RRKM}}(E) = \frac{1}{\bar{s}} \quad (4.13)$$

the inverse mean gap time. In general, the inverse of the mean gap time is

$$k \equiv \frac{1}{\bar{s}} = \frac{\phi(E)}{\rho_+^{\text{C}}} \quad (4.14a)$$

$$= k_f^{\text{RRKM}} \left[\frac{\rho_+(E)}{\rho_+^{\text{C}}(E)} \right] \quad (4.14b)$$

$$\geq k_f^{\text{RRKM}}. \quad (4.14c)$$

The inverse gap time can then be interpreted as the statistical unimolecular reaction rate corrected for the volume of trapped trajectories in the reactant phase space^{16,18,50,51,58}.

C. Reactive flux correlation function

The discussion of reactive fluxes across the phase space dividing surface separating reactant from product and of gap times provides a theoretical framework for analyzing the lifetime distribution of an ensemble of trajectories initiated in the reactant well at constant energy, where the lifetime refers to the time to the first crossing of the dividing surface.

Another approach to isomerization kinetics considers an equilibrium (canonical or microcanonical) ensemble of reactants and products. The regression hypothesis relates the total

relaxation rate for an initial perturbation of the equilibrium populations to the autocorrelation function of spontaneous population fluctuations¹⁹. Standard analysis¹⁹ then provides a relation between the isomerization rate, when the latter exists, and the computationally tractable quantity $\mathcal{K}(t)$ given in terms of the reactive flux across the barrier:

$$\mathcal{K}(t) = \frac{1}{x_+ x_-} \langle \dot{q}(0) \delta[q(0) - q^\ddagger] \Theta_+[q(t)] \rangle \sim \frac{e^{-t/\tau}}{\tau}. \quad (4.15)$$

In this expression, $q \equiv \bar{A}_1$, the reaction coordinate, and the DS is determined by symmetry, so that the critical value $q^\ddagger = 0$. We also have

$$\frac{1}{\tau} = k_f + k_b = 2k_f. \quad (4.16)$$

In our calculations the ensemble average $\langle \dots \rangle$ corresponds to a microcanonical ensemble (average over the entire energy shell Σ_E), Θ_+ is the characteristic function for the configuration space region $\bar{A}_2 > 0$, and equilibrium fractions are $x_+ = x_- = 1/2$. In the limit $t \rightarrow 0$, the right hand side of equation (4.15) is just twice the statistical rate k_f^{RRKM} , eq. (4.12).

Operationally, in principle we must sample the DS without regard to the sign of the initial velocity $\dot{q}(0)$. A trajectory contributes to the average (4.15) at time t :

- (i) Only if the phase point is in the product well ($q > 0$) at time t ,
- (ii) With a sign (\pm) determined by the *initial* sign of \dot{q} .

The right hand side of (4.15) decays to zero as $t \rightarrow \infty$, as trajectories initially crossing from product to reactant ($\dot{q} < 0$) eventually return to the product side, leading to cancellation. If the right hand side of (4.15) exhibits a so-called ‘plateau’ region in which it is approximately constant, followed by exponential decay, then an isomerization rate can be extracted from the computation. This behavior indicates a well-defined separation of timescales: trajectories remain trapped in either well for long times with only infrequent transitions (crossing of the DS) between wells. On the other hand, if the reactive flux correlation functions exhibits oscillatory decay, then no rate constant exists at the energy in question. Pioneering computations of flux correlation functions for a number of 2 DoF dynamical models for isomerization were made by DeLeon and Berne^{15,16}.

In practice, we exploit the symmetry of the potential, and sample only initial conditions with $\dot{\bar{A}}_1 > 0$. If the fraction of the phase points in the product well $A_1 > 0$ at time t is $W(t)$, then the fraction of the phase points in the reactant well, $A_1 < 0$, at time t is $1 - W(t)$.

As the potential is symmetric about $A_1 = 0$, reversing the initial sign of \dot{q} leads to a set of symmetry-related trajectories with the occupancy of the two wells now $1 - W(t)$ and $W(t)$, respectively. Adding the contributions of trajectories to (4.15) with appropriate sign yields a result proportional to $2W(t) - 1$, which can be calculated from $W(t)$ directly.

A connection between the gap time and the reactive flux approaches to isomerization kinetics was established by Straub and Berne in their work on the “absorbing boundary” method for computing isomerization rates^{69,70}. Assuming that there are no correlations between successive crossings of the DS for a given trajectory (i.e., assuming “chaotic” dynamics), then the single-passage gap/lifetime distribution can be used to derive an expression for the reactive flux, and hence the associated isomerization rate⁷⁰.

V. PARAMETER VALUES AND ENERGY SCALES

A. Physical parameters

We study a 2-mode truncation of the dynamics of a silicon nanobeam having rectangular cross section under compressive stress, subject to hinged boundary conditions. The following physical parameter values are used^{9–11}: elastic modulus $Q = 1.3 \times 10^{11}$ J/m³; uncompressed length $L_0 = 5 \times 10^{-8}$ m; width $w = 2 \times 10^{-9}$ m; depth $d = 1 \times 10^{-9}$ m; density $\rho = 2330$ kg/m³. For these parameters, the critical value of the strain ϵ_c , obtained by solving the implicit equation (2.14b), is $\epsilon_c = -0.000329$.

B. Strain values: 3 cases

For a beam described by the physical parameters listed above, we consider the dynamics for 3 values of the compressive stress. The corresponding strain values and associated parameters are given in Table II. Strain values for the three cases are: case I, $\epsilon = -0.00065840 \simeq 2 \times \epsilon_c$; case II, $\epsilon = -0.00197520 \simeq 6 \times \epsilon_c$; case III, $\epsilon = -0.001419692 \simeq 4 \times \epsilon_c$. The strain value for case III is chosen so that the energy of the index 2 saddle lies just above the pair of index 1 saddles at $\beta = -0.0001$.

Contour plots of the potential (2.19) for the 3 cases considered are given in Figure 2.

Setting coordinate $\bar{A}_2 = 0$ in potential (2.19), we obtain a bistable potential which is a function of the ‘reaction coordinate’ \bar{A}_1 . In Table II we give the value of the barrier height ΔE for each of the 3 cases (degrees K). It can be seen that the barrier heights are comparable to thermal energies ~ 100 K for all cases. We have also estimated the magnitude of vibrational quanta $\hbar\omega$ associated with oscillations of the beam along the reaction coordinate at the potential energy minimum; these energies are given in Table II. We have $\hbar\omega/k_B T \ll 1$ for $T \gtrsim 100$ K.

VI. RESULTS AND DISCUSSION

A. Reactive flux, phase space volumes and ergodicity

We have computed reactive fluxes associated with the symmetry-determined DS $\bar{A}_2 = 0$ for each of the 3 cases listed in Table II at 3 energies: $E = 10^{-9}$, $E = 10^{-8}$ and $E = 10^{-7}$. For cases II and III, where the coordinate origin $(0, 0)$ is an index 2 saddle on the potential energy surface flanked by a pair of index 1 saddles, we have also performed computations at several values of $E < 0$. For case II, where the energy of the index 2 saddle is well above the pair of index 1 saddles, we have used 3 additional energies: $E = -2.12 \times 10^{-7}$, $E = -2 \times 10^{-7}$ and $E = -1 \times 10^{-7}$. For case III where the energy of the index 2 saddle is only just above the pair of index 1 saddles we consider 2 additional energies: $E = -4 \times 10^{-9}$ and $E = -2.5 \times 10^{-9}$. In each case the lowest energy is close to the index 1 saddle energy. Our numerical results, obtained via Monte Carlo sampling of the DS, are presented in Tables III–V. For further details on the numerical methods used in these computations, see ref. 55.

Numerical results for mean gap time \bar{s} , reactive flux $\phi_+(E)$, reactant volume $\rho_+^C(E) = \bar{s} \times \phi_+$, reactant density of states $\rho_+(E)$, pulse decay constant κ (see below) and the statistical isomerization rate k_f^{RRKM} for each case and energy studied are given in Tables III–V.

For the simple quartic potential obtained by setting $\bar{A}_1 = 0$, action integrals (fluxes) $I_2(E)$ for motion in the invariant plane Π_2 can be computed explicitly as a function of total energy E in terms of complete Elliptic integrals. These analytical expressions, not reported here, have been used as a check on our numerical calculations.

Our results show that $\rho_+^C(E) < \rho_+(E)$ in all instances; in the majority of cases the phase space volume swept out by reacting (crossing) trajectories is considerably smaller than the full classical density of states associated with the reactant region of phase space. This means that, for the stress values and energies studied here, the buckled nanobeam dynamics is very far from being ergodic. Ergodicity is usually taken to be a necessary (but by no means sufficient) condition for the applicability of statistical theories of reaction rates.

Some representative trajectories for the 3 cases are shown in Figure 3. For each case/energy we present two plots: one shows 20 trajectories initiated on the DS and followed until the first recrossing of the DS, while the other shows a single trajectory followed for 200 crossings of the DS. It is clear by inspection of the single trajectory plots that the

dynamics is far from ergodic on the timescale considered; the trajectories appear to be quasiperiodic or weakly chaotic at most.

B. Gap time distribution

Both gap time distributions $\mathcal{P}(t)$ and associated (unnormalized) lifetime distributions $F(t)$ have been computed for all cases. The functions $\mathcal{P}(t)$ and $\log[F(t)]$ are plotted in Figure 4 for the lowest energy in each case. The results shown represent the range of behavior found for the various cases and energies we have studied.

For case I, $E = 10^{-7}$, the gap time distribution essentially consists of a single ‘pulse’ associated with trajectories that enter the well, exhibit a single turning point in the reaction coordinate, and then exit through the dividing surface DS_- . The smallest gap time is nonzero, reflecting a delay corresponding to the time it takes for a point on the shortest lived trajectory to reach the turning point and then return to the DS. The lifetime distribution of the set of trajectories in the pulse is however well described by a single exponential decay, with a decay rate (denoted κ) that is much faster than either the RRKM rate k_f^{RRKM} or the inverse of the mean gap time.

For cases II and III, the structure of the gap time distribution is more complex, consisting of multiple pulses. Several early pulses have comparable amplitudes, with amplitude not necessarily decreasing monotonically with gap time. In such cases the computation of decay rates for individual pulses is less accurate due to the possibility of overlapping pulses. At long gap times the distribution becomes smooth, with typically nonexponential decay.

Representative pulse decay constants κ are listed in Tables III–V. In all instances $\kappa \gg k_f^{\text{RRKM}}$.

We note that the gap time distributions seen here are reminiscent of the ‘epistrophic’ patterns of ionization times seen in the work of Mitchell and Delos⁷¹.

C. Reactive flux correlation function

The quantity $\mathcal{K}(t)$ (eq. (4.15)) is plotted in Figure 5 for three different cases/energies. The behavior seen in these plots is again typical of all the cases we have examined: $\mathcal{K}(t)$ exhibits oscillatory decay over a much longer timescale than the gap time decay constant κ .

The absence of a ‘plateau’ region means that an isomerization rate constant *does not exist* for our nanobeam model in the physical regime studied.

D. Gap time distribution on the DS

To further explore the isomerization dynamics of the nanobeam, we examine the distribution of gap times on the dividing surface. That is, we plot contours of the gap time s as a function of coordinates (\bar{A}_2, p_2) on DS_+ .

A set of representative plot is shown in Figure 6, corresponding to case I, $E = 10^{-7}$, case II, $E = 10^{-9}$ and case III, $E = 10^{-9}$. Note that the contour plots are invariant with respect to the inversion operation $(\bar{A}_2, p_2) \rightarrow (-\bar{A}_2, -p_2)$. For each case the gap time s is also plotted along the line $p_2 = 0$.

A significant finding is that for case I the gap time is a smooth function of location on the DS; although there appear to be no singularities inside the boundary (NHIM) with divergent gap times, closer examination (not shown here) confirms the existence of a small region near the NHIM (the boundary of the DS) where gap times are longer, presumably associated with second (and later) pulses that do not cross the TS on first approach but bounce back again one (or more) times. The absence of ‘fractal’ patterns such as those seen in previous studies⁵⁴ indicates that the intra-well dynamics is extremely simple for case I.

The gap time contours on the DS for cases II and III show a more typical⁵⁴ fractal arrangement. Initial condition on the DS for which the gap time diverges presumably lie on the stable manifold of either the NHIM or of a periodic orbit confined to the reactant well. By symmetry, trajectories on the line $p_2 = 0$ having divergent gap times must lie on both the stable manifold (in forward time) and unstable manifold (in backward time) of the NHIM, and hence lie on homoclinic orbits.

VII. CONCLUSIONS AND OUTLOOK

In this paper we have studied the classical (Euler-Bernoulli) mechanics of a 2-mode truncation of the dynamics for a buckled nanobeam with rectangular cross section subject to compressive stress. The physical parameters used correspond to a Silicon nanobeam⁶⁻¹¹. In the stress regime studied, the first transverse displacement mode has become unstable, while the second mode is either stable or unstable, depending on the value of the strain. The resulting beam Hamiltonian has the same form as model 2 DoF systems previously studied in chemistry, which describe a bistable reaction (isomerization) coordinate coupled to an additional transverse or ‘bath’ mode.

We have applied methods from reaction rate theory to characterize the nanobeam ‘isomerization’ dynamics. For the beam model considered, the dividing surface separating ‘reactant’ and ‘product’ configurations for the buckled beam is completely determined by symmetry (coordinate $\bar{A}_1 = 0$). Using exponential dichotomies, we have proved that, for a specified range of the energy, the boundary of the associated dividing surface is a Normally Hyperbolic Invariant Manifold (NHIM).

We have computed reactive fluxes, mean gap times and reactant phase space volumes for 5 stress values at several different energies. In all cases the phase space volume swept out by crossing trajectories is considerably less than the reactant density of states, proving that the dynamics is highly nonergodic. The associated gap time distributions consist of single ‘pulses’ of trajectories. Computation of the reactive flux correlation function shows no sign of a plateau region; rather, the flux exhibits oscillatory decay, indicating that, for the 2-mode model in the physical regime considered, a rate constant for isomerization does not exist.

Problems for future work include study of the dynamical influence of additional ‘bath’ modes, and the investigation of quantum effects at low temperatures.

Acknowledgments

PC and SW acknowledge the support of the Office of Naval Research (Grant No. N00014-01-1-0769) and the Leverhulme Trust.

Appendix A: Proof of the Existence of a Normally Hyperbolic Invariant Manifold

Roughly speaking, a normally hyperbolic invariant manifold has the property that, under the dynamics linearized about the invariant manifold, growth rates in directions transverse to the invariant manifold dominate the growth rates of directions tangent to the invariant manifold. (For some background on normally hyperbolic invariant manifolds see refs 72–75. An account of Fenichel’s approach to the theory, as well as some history and examples can be found in ref. 28.) The dynamics on Π_2 are completely integrable. For $\beta > 0$ it consists entirely of periodic orbits, and the growth rates (e.g. Lyapunov exponents) associated with all orbits are all zero. For $\beta < 0$ it consists entirely of periodic orbits, *except* for the saddle point at the origin connected by a pair of homoclinic orbits. The periodic orbits all have zero growth rates, and the saddle point and the homoclinic orbits will be discussed separately. We will show that the growth rates transverse to Π_2 are exponential. Hence they dominate the growth rates tangent to Π_2 .

We linearize (3.10) about Π_2 and evaluate the resulting equations on an arbitrary trajectory on Π_2 . Since Π_2 is a plane, and is described in a global coordinate system, linearization about Π_2 is particularly easy. Coordinates describing the directions normal to Π_2 are (\bar{A}_1, \bar{p}_1) , and Π_2 is defined by $\bar{A}_1 = \bar{p}_1 = 0$ in the four dimensional phase space with coordinates $(\bar{A}_1, \bar{p}_1, \bar{A}_2, \bar{p}_2)$.

Therefore, the linearized dynamics about Π_2 is obtained by retaining terms only linear in (\bar{A}_1, \bar{p}_1) :

$$\dot{\bar{A}}_1 = \bar{p}_1, \tag{A1a}$$

$$\dot{\bar{p}}_1 = -2\bar{A}_1 (\alpha + 4\bar{A}_2^2), \tag{A1b}$$

$$\dot{\bar{A}}_2 = \bar{p}_2, \tag{A1c}$$

$$\dot{\bar{p}}_2 = -8\bar{A}_2 (\beta + 4\bar{A}_2^2). \tag{A1d}$$

The linearized dynamics normal to Π_2 are given by:

$$\dot{\bar{A}}_1 = \bar{p}_1, \tag{A2a}$$

$$\dot{\bar{p}}_1 = -2\bar{A}_1 (\alpha + 4\bar{A}_2^2(t)). \tag{A2b}$$

where $\bar{A}_2^2(t)$ is a component of a trajectory on Π_2 , i.e. it is the \bar{A}_2 component of a trajectory

of:

$$\dot{\bar{A}}_2 = \bar{p}_2, \quad (\text{A3a})$$

$$\dot{\bar{p}}_2 = -8\bar{A}_2 (\beta + 4\bar{A}_2^2). \quad (\text{A3b})$$

We now will show that the linear, nonautonomous equation (A2) has two linearly independent solutions; one exponentially growing in time, and the other exponentially decaying in time. This is accomplished by showing that (A2) has an *exponential dichotomy*, and these conditions will depend on α , β , $\bar{A}_2^2(t)$.

The numbers that are typically used to quantify (linearized) growth rates of trajectories are the Lyapunov exponents. However, for nonautonomous ordinary differential equations exponential dichotomies are often more convenient and facilitate the proof of certain results. A discussion of the relationship between Lyapunov exponents and exponential dichotomies can be found in, e.g., refs 76,77.

a. Exponential Dichotomy First, we will provide some background on the notion of exponential dichotomy that is particular to our situation, i.e. two dimensional time-dependent ordinary differential equations. The standard reference on exponential dichotomies is ref. 29.

Consider the linear ordinary differential equation with time dependent coefficients

$$\dot{\mathbf{x}} = L(t)\mathbf{x}, \quad (\text{A4})$$

where $\mathbf{x} = (x, y)$ and the 2×2 matrix $L(t)$ is a continuous function of t , and suppose $X(t)$ is the fundamental solution matrix of (A4). Let $\|\cdot\|$ denote a matrix norm, such as the maximum of the absolute values of the matrix elements. Then (A4) is said to possess an *exponential dichotomy* if there exists a rank-one projection operator P and constants $K_1, K_2, \alpha_1, \alpha_2 > 0$, such that

$$\|X(t)PX^{-1}(\tau)\| \leq K_1 \exp(-\alpha_1(t-\tau)), \quad t \geq \tau, \quad (\text{A5a})$$

$$\|X(t)(\text{id} - P)X^{-1}(\tau)\| \leq K_2 \exp(\alpha_2(t-\tau)), \quad t \leq \tau. \quad (\text{A5b})$$

The condition that the projection operator P has rank one means that, of the two linearly independent solutions of (A4), one is exponentially growing and one is exponentially decaying.

Verifying that (A2) has an exponential dichotomy requires us to solve for the fundamental solution matrix $X(t)$. In general, this is not possible. Instead, we will use results on "roughness of exponential dichotomies"^{29,78}. The relevant result is as follows. Suppose (A4) has the form:

$$\dot{\mathbf{x}} = (A(t) + B(t)) \mathbf{x}, \quad (\text{A6})$$

and suppose that the equation:

$$\dot{\mathbf{x}} = A(t) \mathbf{x}, \quad (\text{A7})$$

has an exponential dichotomy with constants $K_1, K_2, \alpha_1, \alpha_2$. If

$$\sup_{t \in \mathbb{R}} \|B(t)\| \left(\frac{K_1}{\alpha_1} + \frac{K_2}{\alpha_2} \right) < 1, \quad (\text{A8})$$

then (A6) has an exponential dichotomy with constants $K'_1 = K'_2 = K_3 > 0$ and $\alpha'_1 = \alpha'_2 = \alpha_3 > 0$.

We now apply these ideas to (A2). Rewriting this equation in the form of (A4) gives:

$$\begin{pmatrix} \dot{\bar{A}}_1 \\ \dot{\bar{p}}_1 \end{pmatrix} = \left[\begin{pmatrix} 0 & 1 \\ -2\alpha & 0 \end{pmatrix} + \begin{pmatrix} 0 & 0 \\ -8\bar{A}_2^2(t) & 0 \end{pmatrix} \right] \begin{pmatrix} \bar{A}_1 \\ \bar{p}_1 \end{pmatrix} \quad (\text{A9})$$

We introduce a linear change of coordinates that diagonalizes the first matrix in this expression:

$$\begin{pmatrix} \bar{A}_1 \\ \bar{p}_1 \end{pmatrix} = T \begin{pmatrix} x \\ y \end{pmatrix} \quad (\text{A10})$$

where

$$T = \begin{pmatrix} 1 & 1 \\ \sqrt{-2\alpha} & -\sqrt{-2\alpha} \end{pmatrix}, \quad T^{-1} = \frac{-1}{2\sqrt{-2\alpha}} \begin{pmatrix} -\sqrt{-2\alpha} & -1 \\ -\sqrt{-2\alpha} & 1 \end{pmatrix} \quad (\text{A11})$$

Then (A9) becomes:

$$\begin{pmatrix} \dot{x} \\ \dot{y} \end{pmatrix} = \left[\begin{pmatrix} \sqrt{-2\alpha} & 1 \\ 0 & -\sqrt{-2\alpha} \end{pmatrix} - \frac{1}{\sqrt{-2\alpha}} \begin{pmatrix} 4\bar{A}_2^2(t) & 4\bar{A}_2^2(t) \\ -4\bar{A}_2^2(t) & -4\bar{A}_2^2(t) \end{pmatrix} \right] \begin{pmatrix} x \\ y \end{pmatrix} \quad (\text{A12})$$

First we consider:

$$\begin{pmatrix} \dot{x} \\ \dot{y} \end{pmatrix} = \begin{pmatrix} \sqrt{-2\alpha} & 1 \\ 0 & -\sqrt{-2\alpha} \end{pmatrix} \begin{pmatrix} x \\ y \end{pmatrix} \quad (\text{A13})$$

The fundamental solution matrix is given by:

$$X(t) = \begin{pmatrix} e^{\sqrt{-2\alpha}t} & 0 \\ 0 & e^{-\sqrt{-2\alpha}t} \end{pmatrix} \quad (\text{A14})$$

We take as the projection matrix:

$$P = \begin{pmatrix} 0 & 0 \\ 0 & 1 \end{pmatrix} \quad (\text{A15})$$

Then, using (A15) and (A14), we have:

$$X(t)PX^{-1}(\tau) = \begin{pmatrix} 0 & 0 \\ 0 & e^{-\sqrt{-2\alpha}(t-\tau)} \end{pmatrix} \quad (\text{A16a})$$

and

$$X(t)(\text{id} - P)X^{-1}(\tau) = \begin{pmatrix} e^{\sqrt{-2\alpha}(t-\tau)} & 0 \\ 0 & 0 \end{pmatrix} \quad (\text{A16b})$$

It follows that (A13) has an exponential dichotomy with $K_1 = K_2 = 1$ and $\alpha_1 = \alpha_2 = \sqrt{-2\alpha}$. We now need to check (A8). For (A12) this condition takes the form:

$$\frac{4 \sup_{t \in \mathbb{R}} |\bar{A}_2^2(t)|}{-\alpha} < 1. \quad (\text{A17})$$

The quantity $\sup_{t \in \mathbb{R}} |\bar{A}_2^2(t)|$ is the maximum value that $\bar{A}_2^2(t)$ attains along a trajectory, and this can be precisely computed, as we now show.

In Section III B we showed the the dynamics in the $\bar{A}_2 - \bar{p}_2$ plane is Hamiltonian, with Hamiltonian given by:

$$\bar{H}_2 = \frac{\bar{p}_2^2}{2} + 4\beta\bar{A}_2^2 + 8\bar{A}_2^4. \quad (\text{A18})$$

Trajectories lie on level curves of the Hamiltonian \bar{H}_2 :

$$\frac{\bar{p}_2^2}{2} + 4\beta\bar{A}_2^2 + 8\bar{A}_2^4 = E, \quad (\text{A19})$$

where

$$\begin{aligned} E &\geq 0 & \text{for } \beta &\geq 0, \\ E &> -\frac{1}{2}\beta^2 & \text{for } \beta &< 0. \end{aligned} \quad (\text{A20})$$

The quantity $\sup_{t \in \mathbb{R}} |\bar{A}_2^2(t)|$ corresponds to the largest “turning point” of a trajectory, i.e., the largest value of \bar{A}_2^2 that intersects the \bar{A}_2 axis. An equation for this quantity can be obtained by setting $\bar{p}_2 = 0$ in (A19). Doing so, and rearranging terms, gives the following quadratic equation for \bar{A}_2^2 :

$$\bar{A}_2^4 + \frac{\beta}{2}\bar{A}_2^2 - \frac{E}{8} = 0. \quad (\text{A21})$$

The solution of this equation is:

$$\bar{A}_2^2 = -\frac{\beta}{4} \pm \frac{1}{4}\sqrt{\beta^2 + 2E} \quad (\text{A22})$$

and we will take the plus sign in front of the square root since we are seeking the largest root. It is also useful to note that this expression is an increasing function of E since:

$$\frac{d\bar{A}_2^2}{dE} = \frac{1}{4\sqrt{\beta^2 + 2E}} > 0. \quad (\text{A23})$$

Therefore we seek the largest value of E such that (A17) is satisfied. This is obtained by equating the expression for $\bar{A}_2^2 = -\frac{\beta}{4} + \frac{1}{4}\sqrt{\beta^2 + 2E}$ to $-\frac{\alpha}{4}$, which gives:

$$-\beta + \sqrt{\beta^2 + 2E} = -\alpha. \quad (\text{A24})$$

and then solving this expression for E :

$$E_{\max} = \frac{\alpha^2}{2} \left(1 - 2\frac{\beta}{\alpha} \right). \quad (\text{A25})$$

* gse1@cornell.edu

† stephen.wiggins@mac.com

¹ H. G. Craighead. Nanoelectromechanical systems. *Science*, 290:1532, 2000.

² M. Roukes. Plenty of room indeed. *Scientific American*, 285:48, 2001.

³ M. Blencowe. Quantum electromechanical systems. *Phys. Rep.*, 395:159, 2004.

⁴ B. Lautrup. *Physics of Continuous Matter: Exotic and Everyday Phenomena in the Macroscopic World*. CRC Press, second edition, 2011.

⁵ M. Poot and H. S. J. van der Zant. Mechanical systems in the quantum regime. *Phys. Rep.*, 511(12):273–335, 2012.

⁶ W. E. Lawrence. Phonon description and the Euler buckling instability of a mesoscopic bar at fixed strain. *Physica B*, 316-317:448–451, 2002.

⁷ S. M. Carr, W, and M. N. Wybourne. Buckling cascade of free-standing mesoscopic beams. *Europhys. Lett.*, 69(6):952–958, 2005.

⁸ W. E. Lawrence, M. N. Wybourne, and S. M. Carr. Compressional mode softening and Euler buckling patterns in mesoscopic beams. *New J. Phys.*, 8:223, 2006.

- ⁹ A. Chakraborty, S. Bagchi, and K. L. Sebastian. Buckled nano rod - a two state system and its dynamics. *J. Comput. Theor. Nanosci.*, 4:504, 2007.
- ¹⁰ A. Chakraborty. Buckled nano rod - a two state system and quantum effect on its dynamics. *Molecular Physics*, 107(17):1777–1786, 2009.
- ¹¹ A. Chakraborty. Buckled nano rod - a two state system and quantum effect on its dynamics using system plus reservoir model. *Molecular Physics*, 109(4):517–526, 2011.
- ¹² P. J. Robinson and K. A. Holbrook. *Unimolecular Reactions*. Wiley, New York, 1972.
- ¹³ W. Forst. *Theory of Unimolecular Reactions*. Academic, New York, 1973.
- ¹⁴ D. Chandler. Statistical mechanics of isomerization dynamics in liquids and transition state approximation. *J. Chem. Phys.*, 68:2959–2970, 1978.
- ¹⁵ N. DeLeon and B. J. Berne. Intramolecular rate process: Isomerization dynamics and the transition to chaos. *J. Chem. Phys.*, 75:3495–3510, 1981.
- ¹⁶ B. J. Berne, N. DeLeon, and R. O. Rosenberg. Isomerization Dynamics and the Transition to Chaos. *J. Phys. Chem.*, 86:2166–2177, 1982.
- ¹⁷ M. J. Davis and S. K. Gray. Unimolecular reactions and phase space bottlenecks. *J. Chem. Phys.*, 84:5389–5411, 1986.
- ¹⁸ S. K. Gray and S. A. Rice. Phase space bottlenecks and statistical theories of isomerization reactions. *J. Chem. Phys.*, 86:2020–2035, 1987.
- ¹⁹ D. Chandler. *Introduction to Modern Statistical Mechanics*. Oxford University Press, New York, 1987.
- ²⁰ T. Baer and W. L. Hase. *Unimolecular Reaction Dynamics*. Oxford University Press, New York, 1996.
- ²¹ G. S. Ezra, H. Waalkens, and S. Wiggins. Microcanonical rates, gap times, and phase space dividing surfaces. *J. Chem. Phys.*, 130:164118, 2009.
- ²² P. Pechukas. Transition state theory. *Ann. Rev. Phys. Chem.*, 32:159–177, 1981.
- ²³ H. Waalkens, R. Schubert, and S. Wiggins. Wigner’s dynamical transition state theory in phase space: classical and quantum. *Nonlinearity*, 21:R1–R118, 2008.
- ²⁴ G. S. Ezra and S. Wiggins. Phase-space geometry and reaction dynamics near index 2 saddles. *J. Phys. A*, 42:205101, 2009.
- ²⁵ P. Collins, G. S. Ezra, and S. Wiggins. Index k saddles and dividing surfaces in phase space with applications to isomerization dynamics. *J. Chem. Phys.*, 134:244105, 2011.

- ²⁶ G. Haller, J. Palacian, P. Yanguas, T. Uzer, and C. Jaffé. Transition States Near Rank-Two Saddles: Correlated Electron Dynamics of Helium. *Comm. Nonlinear Sci. Num. Simul.*, 15:48–59, 2010.
- ²⁷ G. Haller, T. Uzer, J. Palacian, P. Yanguas, and C. Jaffé. Transition state geometry near higher-rank saddles in phase space. *Nonlinearity*, 24:527–561, 2011.
- ²⁸ S. Wiggins. *Normally hyperbolic invariant manifolds in dynamical systems*. Springer-Verlag, 1994.
- ²⁹ W. A. Coppel. *Dichotomies in Stability Theory*, volume 629 of *Lecture Notes in Mathematics*. Springer-Verlag, New York, Heidelberg, Berlin, 1978.
- ³⁰ R. Maranganti and P. Sharma. Revisiting quantum notions of stress. *Proc. Roy. Soc. A*, 466:2097–2116, 2010.
- ³¹ J. Carr. *Applications of Centre Manifold Theory*, volume 35 of *Applied Mathematical Sciences*. Springer, New York, 1981.
- ³² R. Temam. *Infinite Dimensional Dynamical Systems in Mechanics and Physics*, volume 68 of *Applied Mathematical Sciences*. Springer, New York, second edition, 1997.
- ³³ F. C. Moon and P. J. Holmes. A magnetoelastic strange attractor. *J. Sound Vibration*, 65:275–296, 1979.
- ³⁴ F. C. Moon and P. J. Holmes. Addendum: A magnetoelastic strange attractor. *J. Sound Vibration*, 69:339, 1980.
- ³⁵ P. J. Holmes and J. E. Marsden. A partial differential equation with infinitely many periodic orbits: chaotic oscillations of a forced beam. *Arch. Rational Mech. Anal.*, 76:135–166, 1981.
- ³⁶ S. Wiggins, L. Wiesenfeld, C. Jaffe, and T. Uzer. Impenetrable barriers in phase-space. *Phys. Rev. Lett.*, 86(24):5478–5481, 2001.
- ³⁷ T. Uzer, C. Jaffe, J. Palacian, P. Yanguas, and S. Wiggins. The geometry of reaction dynamics. *Nonlinearity*, 15:957–992, 2002.
- ³⁸ H. Waalkens and S. Wiggins. Direct construction of a dividing surface of minimal flux for multi-degree-of-freedom systems that cannot be recrossed. *J. Phys. A*, 37:L435–L445, 2004.
- ³⁹ E. Thiele. Comparison of the classical theories of unimolecular reactions. *J. Chem. Phys.*, 36(6):1466–1472, 1962.
- ⁴⁰ V. I. Arnold. *Mathematical Methods of Classical Mechanics*. Springer-Verlag, New York, 1978.
- ⁴¹ J. Binney, O. E. Gerhard, and P. Hut. Structure of surfaces of section. *Mon. Not. Roy. Astron.*

- Soc.*, 215:59–65, 1985.
- ⁴² H-D. Meyer. Theory of the Liapunov exponents of Hamiltonian systems and a numerical study on the transition from regular to irregular classical motion. *J. Chem. Phys.*, 84:3147–3161, 1986.
- ⁴³ M. Toller, G. Jacucci, G. DeLorenzi, and C. P. Flynn. Theory of classical diffusion jumps in solids. *Phys. Rev. B*, 32:2082–2095, 1985.
- ⁴⁴ R. S. MacKay. Flux over a saddle. *Phys. Lett. A*, 145:425–427, 1990.
- ⁴⁵ R. E. Gillilan. Invariant surfaces and phase space flux in 3-dimensional surface diffusion. *J. Chem. Phys.*, 93:5300–5314, 1990.
- ⁴⁶ P. Brumer, D. E. Fitz, and D. Wardlaw. Time delay for bimolecular collisions: Utility of the spectral theorem in the classical limit. *J. Chem. Phys.*, 72(1):386–394, 1980.
- ⁴⁷ E. Pollak. A classical spectral theorem in bimolecular collisions. *J. Chem. Phys.*, 74:6763–6764, 1981.
- ⁴⁸ H. Waalkens, A. Burbanks, and S. Wiggins. Efficient procedure to compute the microcanonical volume of initial conditions that lead to escape trajectories from a multidimensional potential well. *Physical Review Letters*, 95:084301, 2005.
- ⁴⁹ H. Waalkens, A. Burbanks, and S. Wiggins. A formula to compute the microcanonical volume of reactive initial conditions in transition state theory. *J. Phys. A*, 38:L759–L768, 2005.
- ⁵⁰ W. L. Hase, D. G. Buckowski, and K. N. Swamy. Dynamics of ethyl radical decomposition. 3. Effect of chemical activation vs microcanonical sampling. *J. Phys. Chem.*, 87:2754–2763, 1983.
- ⁵¹ M. Berblinger and C. Schlier. How accurate is the Rice-Ramsperger-Kassel-Marcus theory? The case of H_3^+ . *J. Chem. Phys.*, 101:4750–4758, 1994.
- ⁵² S. Yu. Grebenshchikov, R. Schinke, and W. L. Hase. State-specific dynamics of unimolecular dissociation. In N. J. B. Greene, editor, *Unimolecular Kinetics: Part 1. The Reaction Step*, volume 39 of *Comprehensive Chemical Kinetics*, pages 105–242. Elsevier, New York, 2003.
- ⁵³ J. N. Stember and G. S. Ezra. Fragmentation kinetics of a Morse oscillator chain under tension. *Chem. Phys.*, 337:11–32, 2007.
- ⁵⁴ H. Waalkens, A. Burbanks, and S. Wiggins. Phase space conduits for reaction in multidimensional systems: HCN isomerization in three dimensions. *J. Chem. Phys.*, 121(13):6207–6225, 2004.
- ⁵⁵ P. Collins, G. S. Ezra, and S. Wiggins. Phase space structure and dynamics for the Hamiltonian isokinetic thermostat. *J. Chem. Phys.*, 133:014105, 2010.

- ⁵⁶ N. B. Slater. New Formulation of Gaseous Unimolecular Dissociation Rates. *J. Chem. Phys.*, 24(6):1256–1257, 1956.
- ⁵⁷ N. B. Slater. *Theory of Unimolecular Reactions*. Cornell University Press, Ithaca, NY, 1959.
- ⁵⁸ R. S. Dumont and P. Brumer. Dynamic theory of statistical unimolecular decay. *J. Phys. Chem.*, 90:3509–3516, 1986.
- ⁵⁹ B. K. Carpenter. Nonexponential decay of reactive intermediates: new challenges for spectroscopic observation, kinetic modeling and mechanistic interpretation. *J. Phys. Org. Chem.*, 16:858–868, 2003.
- ⁶⁰ D. L. Bunker. Monte Carlo calculation of triatomic dissociation rates. I. N_2O and O_3 . *J. Chem. Phys.*, 37:393–403, 1962.
- ⁶¹ D. L. Bunker. Monte Carlo calculations. IV. Further studies of unimolecular dissociation. *J. Chem. Phys.*, 40:1946–1957, 1964.
- ⁶² D. L. Bunker and W. L. Hase. Non-RRKM unimolecular kinetics: molecules in general, and CH_3NC in particular. *J. Chem. Phys.*, 59:4621–4632, 1973.
- ⁶³ E. Thiele. Comparison of the classical theories of unimolecular reactions. II. A model calculation. *J. Chem. Phys.*, 38(8):1959–1966, 1963.
- ⁶⁴ D. L. Bunker. *Theory of Elementary Gas Reaction Rates*. Pergamon, Oxford, 1966.
- ⁶⁵ D. L. Bunker and M. L. Pattengil. Monte Carlo calculations. VI A re-evaluation of RRKM theory of unimolecular reaction rates. *J. Chem. Phys.*, 48:772–776, 1968.
- ⁶⁶ W. L. Hase. Dynamics of Unimolecular Reactions. In W. H. Miller, editor, *Modern Theoretical Chemistry*, volume 2, pages 121–170. Plenum, New York, 1976.
- ⁶⁷ Lourderaj U. and W. L. Hase. Theoretical and computational studies of unimolecular reaction dynamics. *J. Phys. Chem. A*, 113:2236–2253, 2009.
- ⁶⁸ W. Forst. *Unimolecular Reactions*. Cambridge University Press, Cambridge, 2003.
- ⁶⁹ J. E. Straub and B. J. Berne. A rapid method for determining rate constants via molecular dynamics. *J. Chem. Phys.*, 83:1138–1139, 1985.
- ⁷⁰ J. E. Straub and B. J. Berne. On determining reaction kinetics by molecular dynamics using absorbing barriers. *J. Phys. Chem.*, 89:5188–5191, 1985.
- ⁷¹ J.B. Delos and K.A. Mitchell. Fractal structure in ionization dynamics. *Few-Body Systems*, 38:181–185, 2006.
- ⁷² N. Fenichel. Persistence and smoothness of invariant manifolds for flows. *Ind. Univ. Math. J.*,

21:193–225, 1971.

- ⁷³ N. Fenichel. Asymptotic stability with rate conditions. *Ind. Univ. Math. J.*, 23(1109-1137), 1974.
- ⁷⁴ N. Fenichel. Asymptotic stability with rate conditions, ii. *Ind. Univ. Math. J.*, 26:81–93, 1977.
- ⁷⁵ M. W. Hirsch, C. C. Pugh, and M. Shub. *Invariant Manifolds*, volume 583 of *Lecture Notes in Mathematics*. Springer, New York, 1977.
- ⁷⁶ L. Dieci, R. D. Russell, and E. S. Van Vleck. On the computation of Lyapunov exponents for continuous dynamical systems. *SIAM J. Numer. Anal.*, 34(1):402–423, 1997.
- ⁷⁷ L. Dieci and E. S. Van Vleck. Lyapunov spectral intervals: Theory and computation. *SIAM J. Numer. Anal.*, 40(2), 2002.
- ⁷⁸ N. Ju and S. Wiggins. On roughness of exponential dichotomy. *Journal of Mathematical Analysis and Applications*, 262:39–49, 2001.

Equilibrium point	Eigenvalues	Energy of the equilibrium
$(\bar{A}_1, \bar{p}_1, \bar{A}_2, \bar{p}_2) = (0, 0, 0, 0)$	$\pm\sqrt{-2\alpha}, \pm 2\sqrt{-2\beta}$	0
$(\bar{A}_1, \bar{p}_1, \bar{A}_2, \bar{p}_2) = (\pm\sqrt{-\alpha}, 0, 0, 0)$	$\pm 2\sqrt{\alpha}, \pm 2\sqrt{2(\alpha - \beta)}$	$-\frac{1}{2}\alpha^2$
$(\bar{A}_1, \bar{p}_1, \bar{A}_2, \bar{p}_2) = (0, 0, \pm\frac{\sqrt{-\beta}}{2}, 0)$	$\pm 4\sqrt{\beta}, \pm\sqrt{2(\beta - \alpha)}$	$-\frac{1}{2}\beta^2$

TABLE I: The location of the equilibria, the eigenvalues of the matrix associated with the linearization of Hamilton's equations about the equilibria, and the (total) energy of the equilibrium. In the last two rows both equilibrium points have the same four eigenvalues.

Case	ϵ	$\bar{\epsilon}$	α	β	$\Delta E/k_B$ [K]	$\hbar\omega/k_B$ [K]
I	-0.00065840	-0.00032942	-0.00032898	0.00065928	50.98	0.092
II	-0.00197520	-0.00033029	-0.00164491	-0.00065404	1274.4	0.206
III	-0.00141969	-0.00032992	-0.00108977	-0.00010000	559.4	0.168

TABLE II: Strain values ϵ and associated parameter values $\bar{\epsilon}$, α and β for the 3 cases used in our computations. Also shown are barrier heights ΔE and estimates of the size of vibrational quanta for beam oscillations about the energy minimum (degrees K).

Energy	\bar{s}	$\phi_+(E)$	$\rho_+^C(E)$	$\rho_+(E)$	$k = \bar{s}^{-1}$	k_f^{RRKM}	κ
1e-09	357.460	0.00000009	0.000031	0.00085	0.00280	0.0001013	0.0254
1e-08	266.663	0.00000086	0.000230	0.00103	0.00375	0.0008351	0.0248
1e-07	174.982	0.00000832	0.001456	0.00210	0.00571	0.0039613	0.0224

TABLE III: Computational results for case I: $\alpha = -0.00032898$, $\beta = 0.00065928$. For discussion see Sec. VI.

Energy	\bar{s}	$\phi_+(E)$	$\rho_+^C(E)$	$\rho_+(E)$	$k = \bar{s}^{-1}$	k_f^{RRKM}	κ
-2.12e-07	7729.396	0.00000023	0.001789	0.00897	0.00013	0.0000258	0.0645
-2e-07	1258.603	0.00000172	0.002160	0.00914	0.00079	0.0001878	0.0406
-1e-07	385.348	0.00001488	0.005734	0.01034	0.00260	0.0014386	0.0481
1e-09	166.588	0.00003186	0.005308	0.01137	0.00600	0.0028028	0.0312
1e-08	165.124	0.00003384	0.005588	0.01132	0.00606	0.0029886	0.0454
1e-07	141.782	0.00004771	0.006764	0.01183	0.00705	0.0040325	0.0492

TABLE IV: Computational results for case II: $\alpha = -0.00164491$, $\beta = -0.00065404$. For discussion see Sec. VI.

Energy	\bar{s}	$\phi_+(E)$	$\rho_+^C(E)$	$\rho_+(E)$	$k = \bar{s}^{-1}$	k_f^{RRKM}	κ
-4e-09	4076.711	0.00000032	0.001308	0.00574	0.00025	0.0000559	0.0618
-2.5e-09	1567.930	0.00000083	0.001304	0.00579	0.00064	0.0001436	0.0427
1e-09	502.955	0.00000236	0.001187	0.00590	0.00199	0.0004001	0.0402
1e-08	307.775	0.00000497	0.001528	0.00600	0.00325	0.0008280	0.0621
1e-07	195.281	0.00001941	0.003791	0.00680	0.00512	0.0028533	0.0410

TABLE V: Computational results for case III: $\alpha = -0.00108977$, $\beta = -0.0001$. For discussion see Sec. VI.

Figure captions

FIG. 1: Phase space portraits in the invariant $\bar{A}_2 - \bar{p}_2$ plane. (a) $\beta > 0$ (b) $\beta < 0$.

FIG. 2: Contour plots of the 2-mode nanobeam potential eq. (3.8) for the 3 compressive stress values considered in this paper. The contour values shown include the particular energies at which the dynamics was studied. (a) $\alpha = -0.00032898$, $\beta = 0.00065928$; (b) $\alpha = -0.00164491$, $\beta = -0.00065404$; (c) $\alpha = -0.00108977$, $\beta = -0.0001$.

FIG. 3: Plots of trajectories initiated on the DS. (a), (b) Case I, energy $E = 10^{-7}$; (c), (d) case II, energy $E = 10^{-9}$; (e), (f) case III, energy $E = 10^{-9}$. Panels (a), (c) and (e) each show 20 trajectories followed until the first recrossing of the DS, while panels (b), (d) and (f) show single trajectories followed for 200 crossings of the DS.

FIG. 4: Gap time distribution $\mathcal{P}(t)$ and the logarithm of the associated (unnormalized) lifetime distribution $F(t)$. (a), (b) case I, energy $E = 10^{-7}$; (c), (d) case II, energy $E = 10^{-9}$; (e), (f) case III, energy $E = 10^{-9}$.

FIG. 5: Reactive flux correlation function $\mathcal{K}(t)$ versus t . (a) case I, energy $E = 10^{-7}$; (b) case II, energy $E = 10^{-9}$; (c) case III, energy $E = 10^{-9}$.

FIG. 6: Contours of the gap time s as a function of coordinates (\bar{A}_2, p_2) on the dividing surface DS_+ (panels (a), (c), (e)) and as a function of \bar{A}_2 along the line $p_2 = 0$ (panels (b), (d) and (e)). (a), (b) case I, energy $E = 10^{-7}$; (c), (d) case II, energy $E = 10^{-9}$; (e), (f) case III, energy $E = 10^{-9}$.

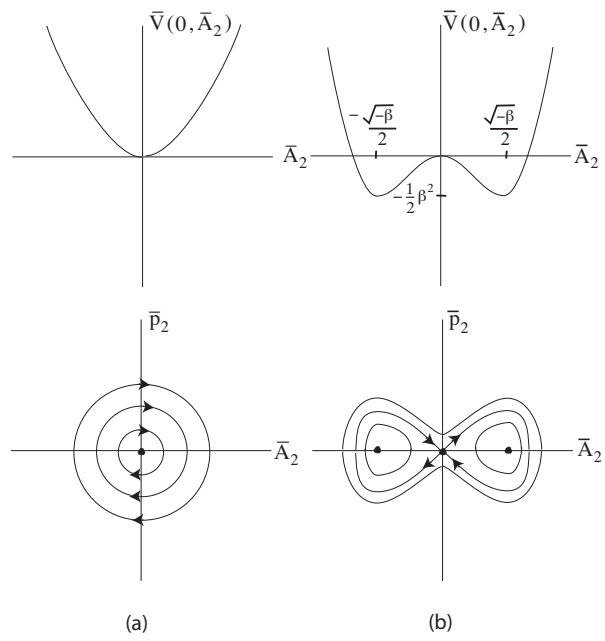


FIGURE 1

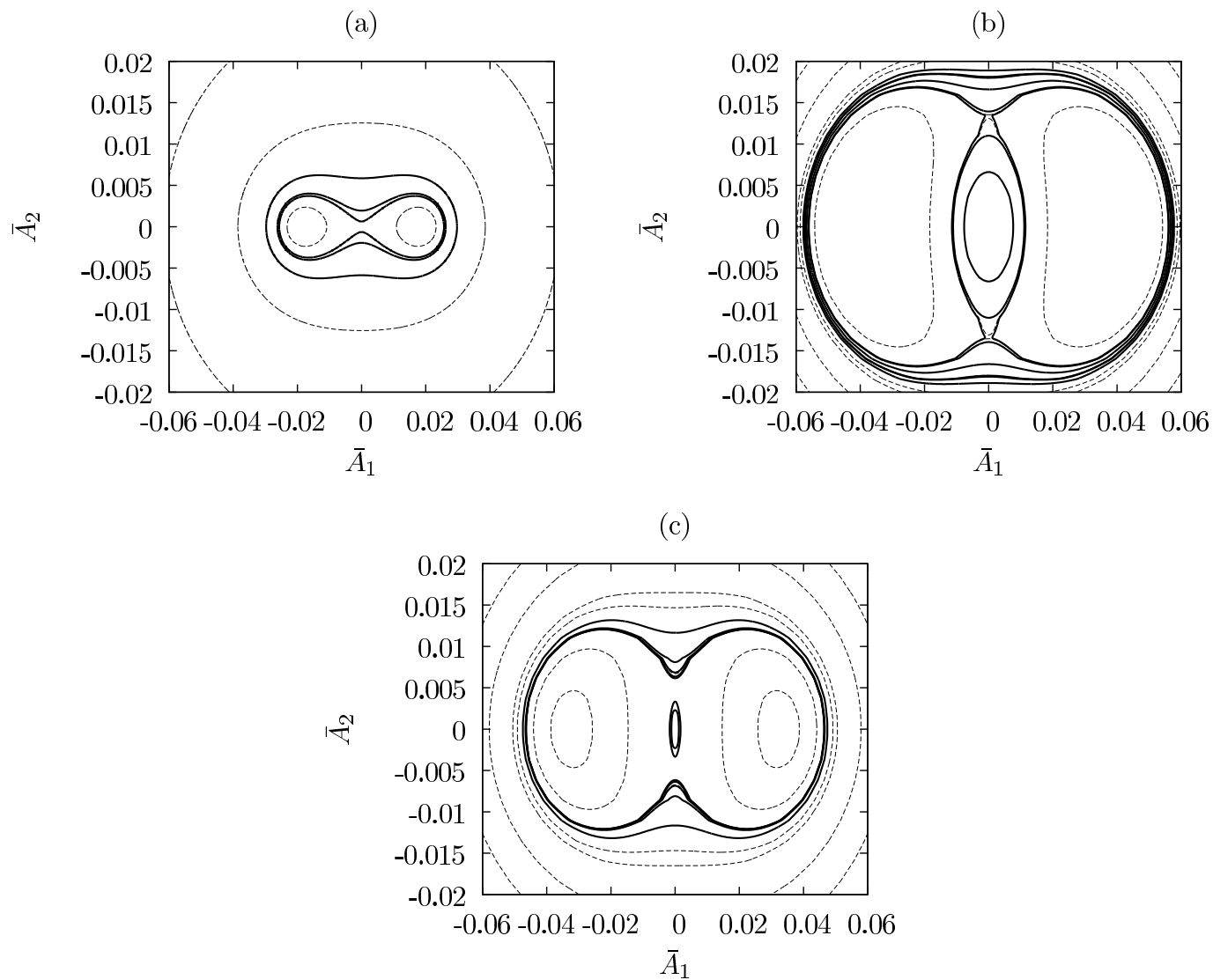


FIGURE 2

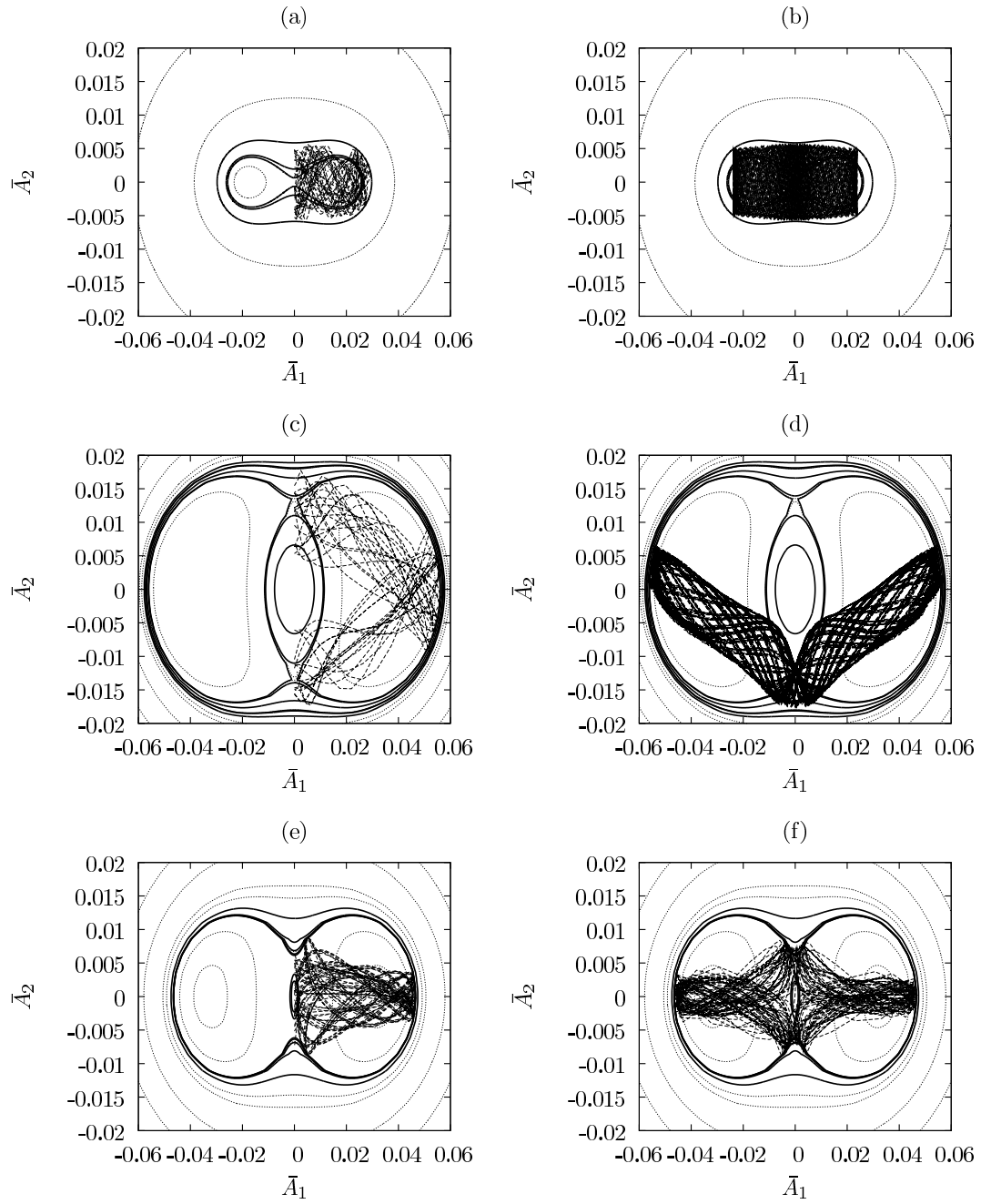


FIGURE 3

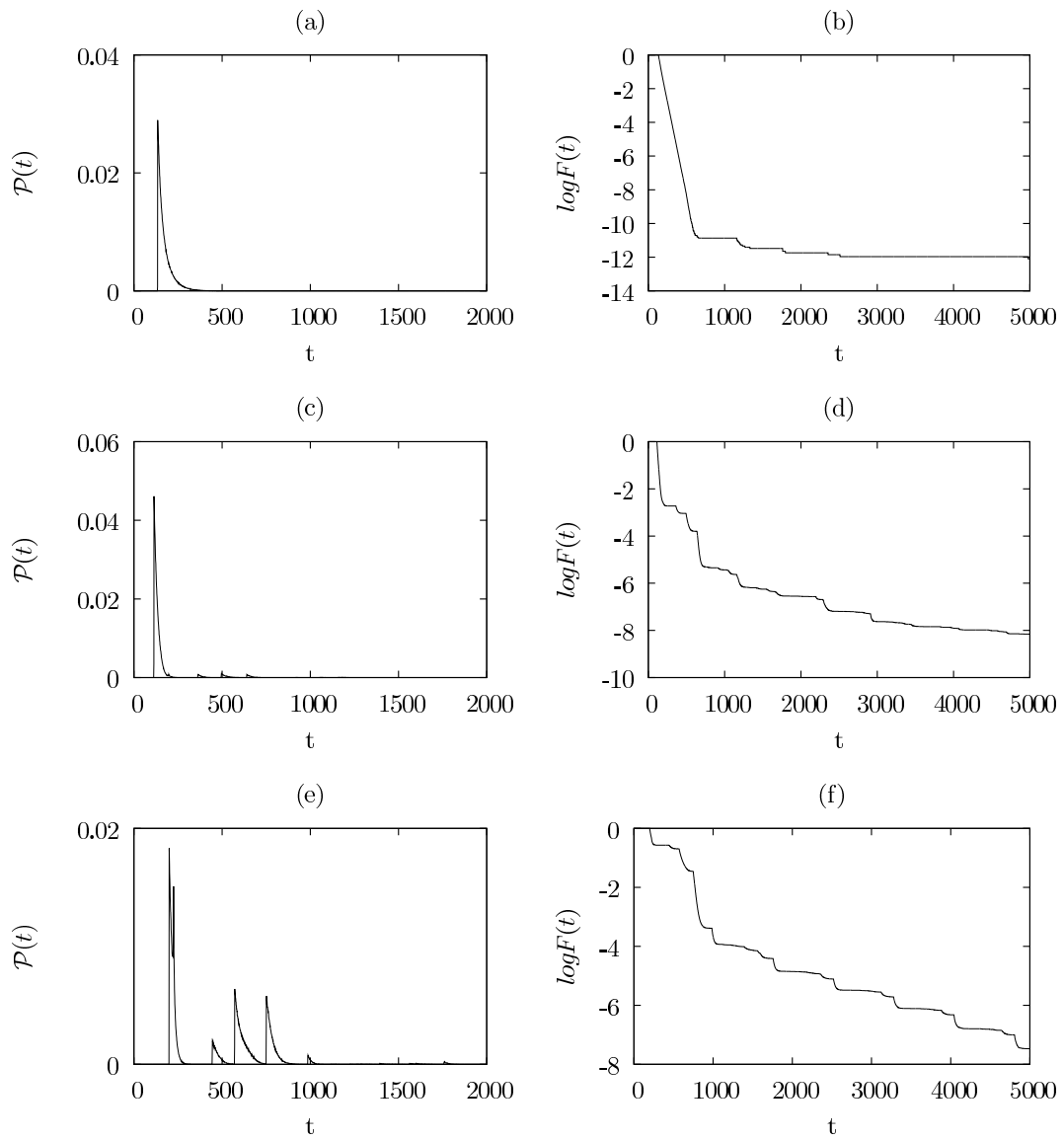


FIGURE 4

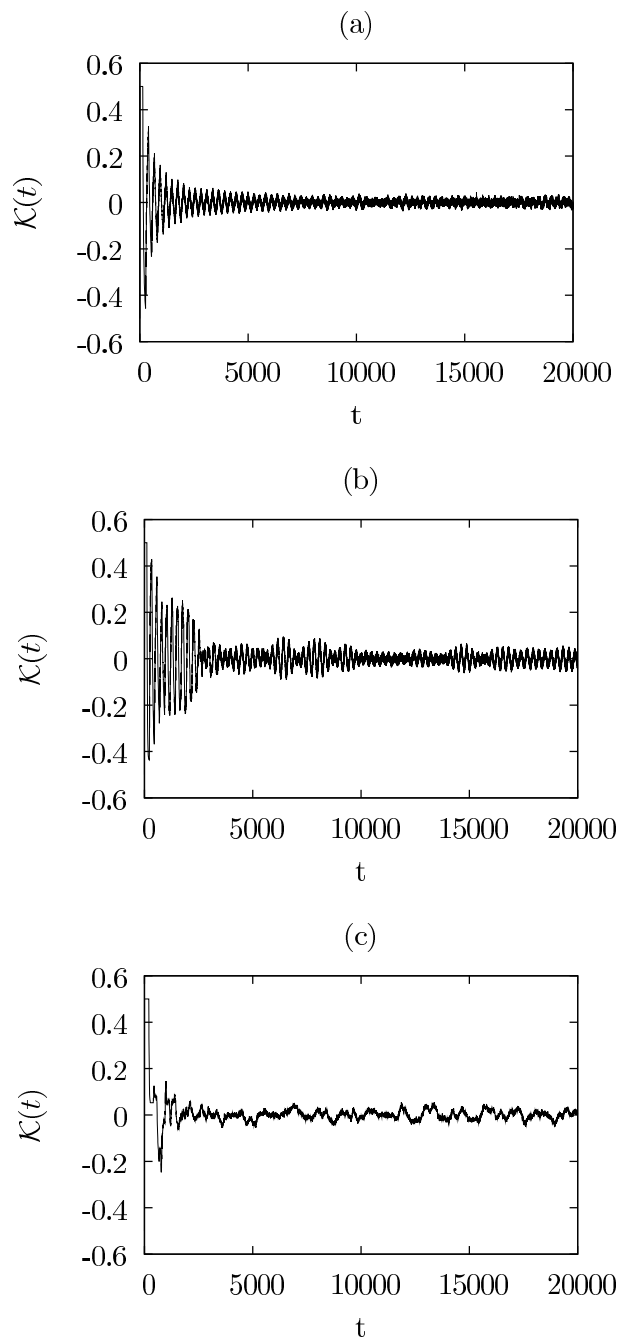


FIGURE 5

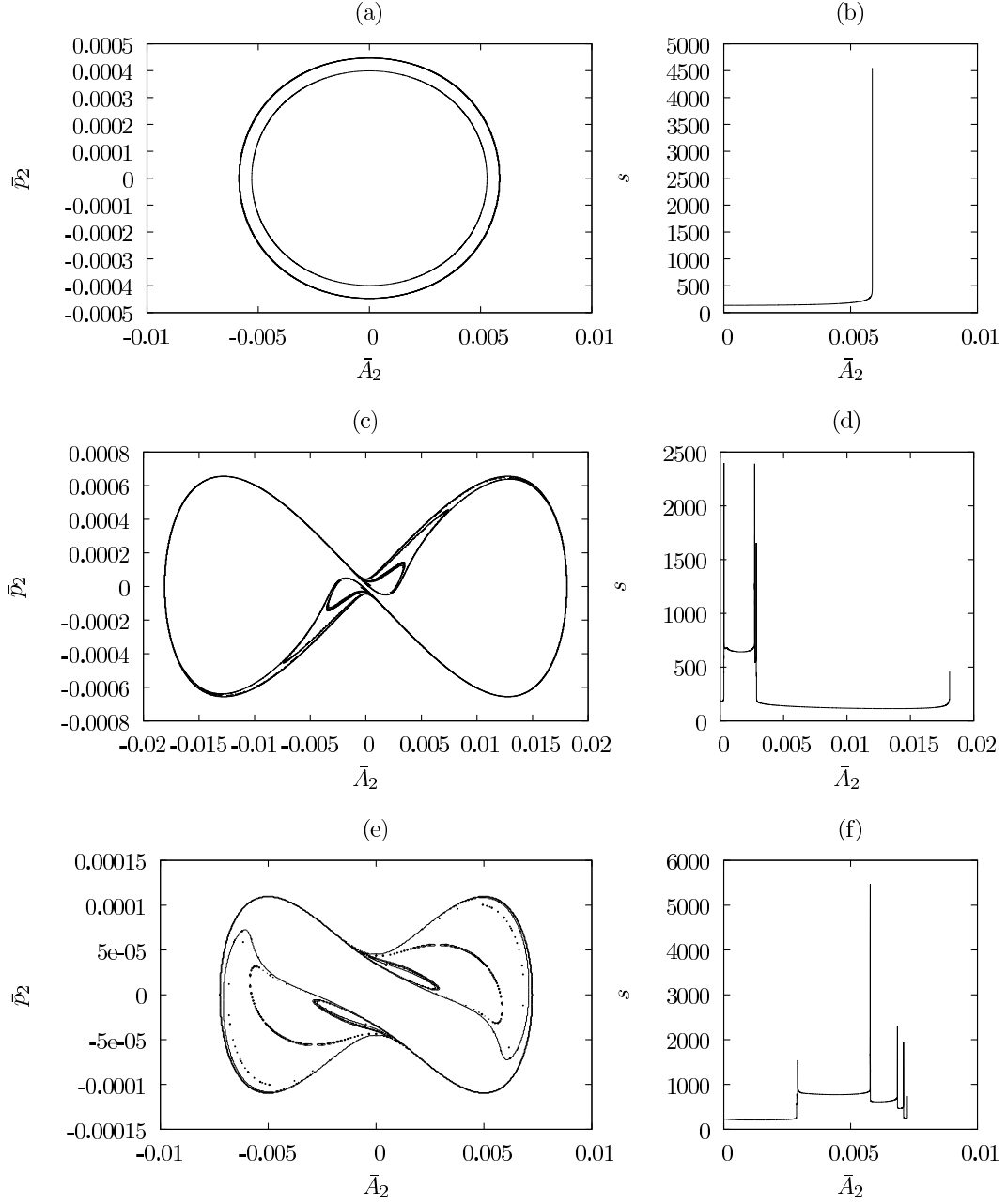


FIGURE 6